small
NANO MICRO

Plasmonic Nickel Nanoantennas

*Jianing Chen, Pablo Albella, Zhaleh Pirzadeh, Pablo Alonso-González, Florian Huth, Stefano Bonetti, Valentina Bonanni, Johan Åkerman, Josep Nogués, Paolo Vavassori, Alexandre Dmitriev, Javier Aizpurua, and Rainer Hillenbrand**

The fundamental optical properties of pure nickel nanostructures are studied by far-field extinction spectroscopy and optical near-field microscopy, providing direct experimental evidence of the existence of particle plasmon resonances predicted by theory. Experimental and calculated near-field maps allow for unambiguous identification of dipolar plasmon modes. By comparing calculated near-field and far-field spectra, dramatic shifts are found between the near-field and far-field plasmon resonances, which are much stronger than in gold nanoantennas. Based on a simple damped harmonic oscillator model to describe plasmonic resonances, it is possible to explain these shifts as due to plasmon damping.

1. Introduction

Optical antennas are devices designed to efficiently convert optical radiation into localized energy, and vice versa.[1–3] They enhance the interaction between light and matter, and hence hold great promise for applications in physics and chemistry, such as in surface-enhanced Raman spectroscopy,[4,5] single molecular fluorescence,[6] nanometric optical trapping,[7] biosensing,[8,9] directing of radiation at optical frequency,[10–12] optical photolithography,[13,14] and laser applications.[15] Currently, there is great interest in the development of nanostructures that possess additional physical properties that allow combining the optical properties of plasmonic antennas with other structural, electronic, or magnetic properties, thus providing multifunctionality in a single device.[16,17] Particularly interesting are nanoantennas made of ferromagnetic materials because they combine an optical plasmon resonance with strong magnetic properties.[18,19]

Dr. J. Chen, Dr. P. Albella, Dr. P. Alonso-González, F. Huth, Prof. P. Vavassori, Prof. R. Hillenbrand
CIC nanoGUNE Consolider
20018 Donostia-San Sebstián, Spain
E-mail: r.hillenbrand@nanogune.eu

Dr. J. Chen, Dr. P. Albella, Dr. J. Aizpurua
Centro de Fisica de Materiales (CSIC-UPV/EHU) and
Donostia International Physics Center (DIPC)
20018 Donostia-San Sebastián, Spain

Dr. Z. Pirzadeh, Dr. V. Bonanni, Prof. A. Dmitriev
Department of Applied Physics
Chalmers University of Technology
41296 Gothenburg, Sweden

Prof. J. Åkerman
Department of Physics
University of Gothenburg
412 96 Gothenburg, Sweden

Dr. S. Bonetti, Dr. V. Bonanni, Prof. J. Åkerman
Materials Physics
Royal Institute of Technology (KTH)
Electrum 229, 164 40 Kista, Sweden

Prof. J. Nogués
CIN2(ICN-CSIC) and Universitat Autónoma de Barcelona
Catalan Institute of Nanotechnology (ICN)
Campus UAB
08193 Bellaterra (Barcelona), Spain

Prof. J. Nogués
Institució Catalana de Recerca i Estudis Avançats (ICREA)
Barcelona, Spain

Prof. P. Vavassori, Prof. R. Hillenbrand
IKERBASQUE
Basque Foundation for Science
48011 Bilbao, Spain

F. Huth
Neaspec GmbH
Bunsenstrasse 5, 82152 Munich, Germany

DOI: 10.1002/smll.201100640

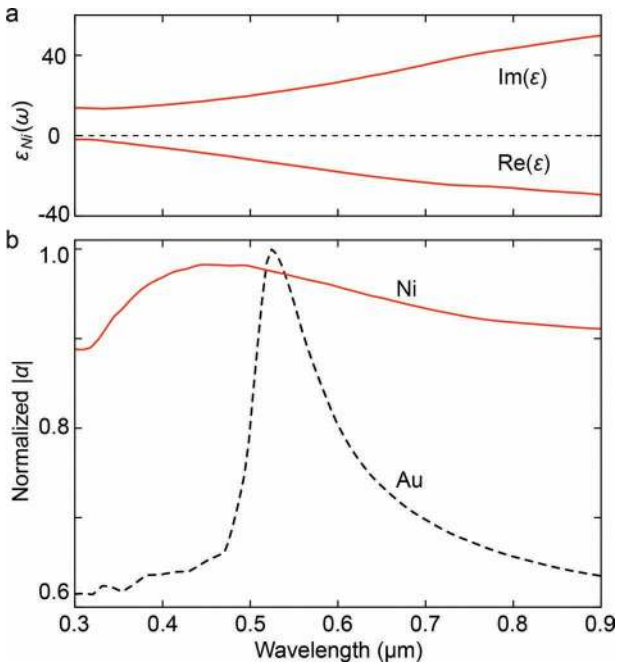

Figure 1. a) Dielectric function of nickel taken from Palik.[25] b) Comparison of the polarizibility $|\alpha|$ of nickel and gold spheres.

The magnetic behavior can open up the pathway to design new types of biosensors, which can be remotely controlled by external magnetic fields. However, plasmons in ferromagnetic materials are typically assumed to exhibit a stronger damping than in noble metals such as gold. A common strategy to overcome this excess damping is to develop hybrid structures consisting of noble metals and ferromagnetic materials, where the noble metal increases the plasmon response.[20–23] These hybrid structures show indeed plasmon-enhanced magneto-optical activity, however, the synthesis requires more tedious fabrication processes. Plasmon properties of pure ferromagnetic nanostructures are a widely unexplored terrain, although they offer the advantage of stronger magnetic polarization and less demanding fabrication.

In order to estimate theoretically the optical properties of pure nickel nanoparticles, the polarizibility $\alpha = 4\pi a^3(\varepsilon_{Ni}\text{-}1)/(\varepsilon_{Ni}\text{+}2)$ of a nickel sphere with radius a and dielectric function ε_{Ni} is calculated. In quasi-electrostatic approximation ($a << \lambda$), the field enhancement is proportional to α_{Ni}.[24] Using dielectric data of nickel (**Figure** 1a) from literature,[25] we plot α_{Ni} as a function of the wavelength and normalize it to its maximum value. We find a resonance (Figure 1b, red solid line) at around 450 nm. Compared to the polarizibility of noble metals such as a gold sphere of equal size (Figure 1b, black dashed line α_{Au}), the nickel resonance is weaker owing to the large imaginary part of its dielectric function. However, the plasmon resonance is still a significant optical feature of nickel nanoparticles, which we explore and verify experimentally in this study. We identify localized plasmon resonances in circular and elliptical nickel nanoantennas employing near-field microscopy and far-field extinction spectroscopy and discuss the surprisingly large shift between far-and near-field spectra.

2. Results and Discussion

Nickel nanoantennas of different sizes and shapes were fabricated on glass substrates by hole–mask colloidal lithography.[26] This method allows the large-area bottom-up fabrication of short-range ordered nanostructures. Before characterizing the plasmonic properties of nickel nanostructures, we verified their ferromagnetic functionality by measuring the magneto-optical Kerr effect (MOKE) as a function of an external magnetic field.[27] The observed hysteresis loops of the disks and elliptical disks clearly reveal the ferromagnetic nature of the nanostructures. (**Figure 2**)

Near-field imaging of the antenna modes was performed with a scattering-type scanning near-field optical microscope (*s*-SNOM) from Neaspec GmbH (www.neaspec.com), operating at λ = 633 nm. (**Figure 3**) Being equipped with a pseudo-heterodyne interferometric detection scheme,[28] the microscope allows for mapping both the amplitude E and phase ϕ of the out-of-plane (normal to the sample surface) electric near-field component at the antenna surface. The combined information of amplitude and phase of this near-field component provides a qualitative description of the surface charge density distribution associated with the plasmon oscillations, and thus allows for unambiguous mode identification.[29]

In **Figure 4** we provide experimental evidence of dipolar plasmon modes in circular and elliptical nickel nanoantennas. The far-field extinction spectrum (Figure 4a) of the 200 nm disks exhibits a clear resonance peak at around λ = 650 nm. In order to identify the mode associated with the resonance peak, we image amplitude and phase (Figure 4b,c) of the

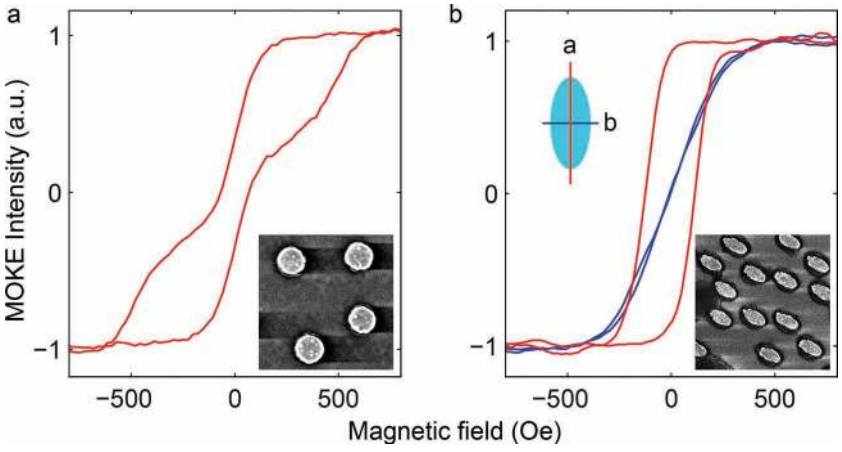

Figure 2. a) MOKE hysteresis loops of nickel disks (diameter = 200 nm); b) MOKE hysteresis loops of elliptical nickel disks (long axis length a = 300 nm, short axis length b = 190 nm). The red and blue curves correspond to the easy and hard magnetization axes of elliptical nickel antennas. Scanning electronic microscopy (SEM) images are shown as insets.

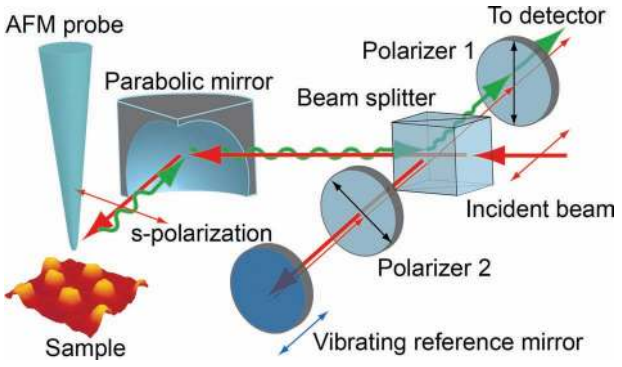

Figure 3. Scattering-type scanning near-field optical microscope (*s*-SNOM). The basis is an atomic force microscope (AFM) that uses cantilevered tips as near-field probes. The incoming light is s-polarized. The p-polarized backscattered light is recorded with a pseudo-heterodyne Michelson interferometer,[28] yielding both the amplitude E and phase ϕ of the vertical (out-of-plane) near-field component.

out-of-plane near-field component. In the amplitude image we observe two bright spots aligned along the polarization direction, which are oscillating out of phase for 180°. Such a near-field pattern provides direct experimental evidence of a dipole mode, which has been reported earlier for plasmon-resonant gold disks.[30,31] A numerical finite-difference time-domain (FDTD) calculation (Lumerical Solutions) of the out-of-plane near-field component (Figure 4d) fully confirms the dipolar plasmon mode observed in the near-field images.

For elliptical nickel disks (middle and right-hand-side columns of Figure 4) we find a strongly anisotropic plasmon response. For a polarization parallel to the short axis (b = 190 nm), far-field extinction spectroscopy (Figure 4a, mid-column) reveals a resonance at around λ = 700 nm, which shifts to 1500 nm for a polarization parallel to the long axis (a = 300 nm). The near-field amplitude and phase images taken at λ = 633 nm (Figure 4b and c mid-column) reveal

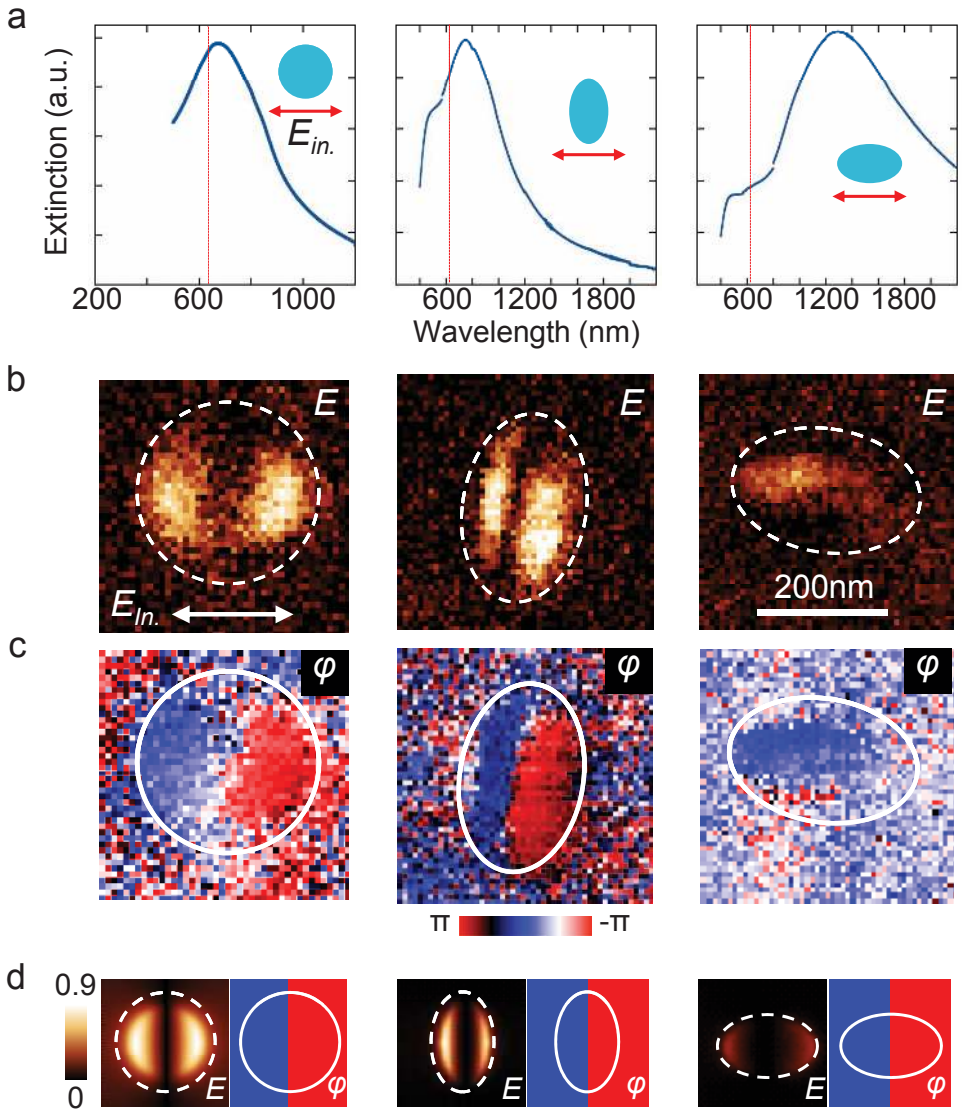

Figure 4. a) Normalized extinction spectra of 200 nm diameter nickel disks (left), of elliptical nickel disks with polarization along the short axis (b = 190 nm, center), and of elliptical nickel disks with polarization along the long axis (a = 300 nm, right). The red lines in the spectra mark the near-field imaging wavelength. b) Near-field amplitude images. The arrow and bar denote the polarization of incident laser beam and the scale of the images, respectively. c) Near-field phase images. d) FDTD-calculated near-field amplitude $E = E_{loc}/E_{in}$ and phase ϕ maps at 633 nm. The white circles in the near-field amplitude and phase images indicate the nickel antennas.

a clear dipolar mode for a polarization along the short axis (commonly referred to as the 'transverse' plasmon mode[32]), where the impinging wavelength is close to the plasmon resonance (central column). Comparison with the calculated near-field distribution (Figure 4d, mid-column) shows an excellent agreement and confirms the dipolar nature of the transverse plasmon mode. The experimental dipolar pattern vanishes when the elliptical antennas are rotated for 90° (right column), as now the imaging wavelength (633 nm) is off resonance (Figure 4b and c right column). This observation shows that the near fields are stronger for polarization parallel to the short axis of the elliptical disks, and provides direct experimental evidence that the near-field strength on the nickel antennas is given by the plasmon excitation rather than by a lightening rod effect. The calculated near-field images (Figure 4d, right column) confirm that the longitudinal plasmon fields are much weaker compared to the transverse mode on resonance (Figure 4d mid-column). The weak longitudinal dipole mode, however, cannot be identified in the experimental image, which exhibits a homogeneous near-field amplitude and phase contrast. We attribute the homogeneous amplitude and phase signal to the near-field material contrast between nickel and glass substrate. This contrast can be explained simply by a weak near-field interaction between tip and sample, which is not taken into account in the numerical calculations.

In order to gain more detailed insights into the plasmon resonance of nickel antennas, we study nickel disks of different diameters. The far-field extinction spectra (**Figure 5**a) show that the plasmon resonance shifts to longer wavelengths with increasing size, which is similar to the size-dependent resonance shifts in noble metal nanoantennas.[33] For the 100 nm and 200 nm disks, we find the same amplitude and phase patterns as in Figure 4. From the near-field images of amplitude and phase (Figure 5c,d) we can thus assign to each resonance peak a dipolar plasmon mode. For the 60 nm diameter disks, the imaging wavelength of 633 nm is strongly off resonance. The near fields are weak and distinct dipolar near-field patterns are observed only on a few disks. An interesting observation is made when we compare the near-field images of the 100 and 200 nm diameter disks. The near-field amplitude signals are nearly equally strong for both samples, even though the imaging wavelength of 633 nm is nearly on resonance for the 200 nm diameter disks but off resonance for the 100 nm diameter disks (see the extinction spectra in Figure 5a). This finding

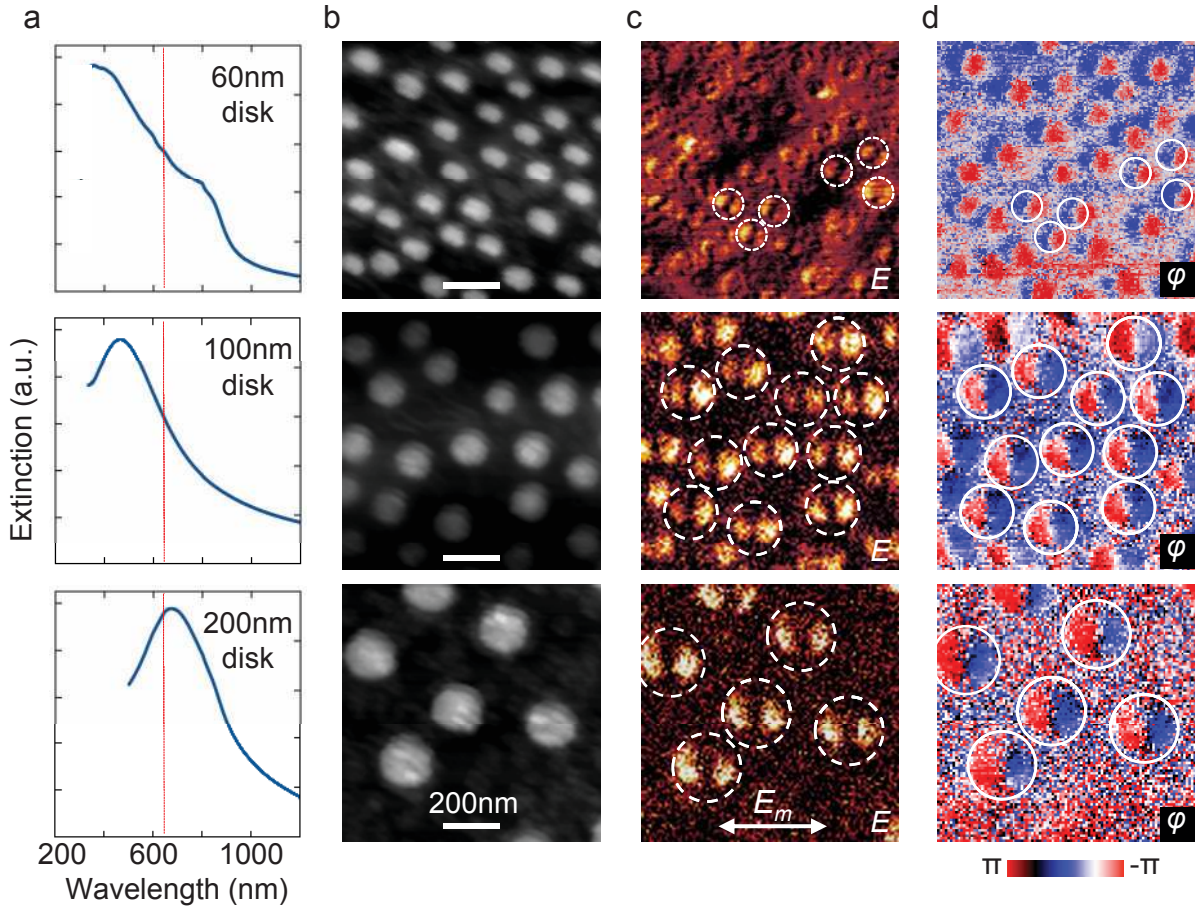

Figure 5. a) Normalized extinction spectra of nickel disks of diameters d = 60, 100, 200 nm, respectively. The red lines in the spectra mark the near-field imaging wavelength. b) Topography images. The elliptical shape of the 60 nm disk is due to sample drift during imaging. c) Near-field amplitude images. d) Near-field phase images. The white circles in the near-field amplitude and phase images indicate the positions of nickel disks.

small NANO MICRO

indicates significant differences between the far- and near-field spectral response of plasmonic nanostructures,[33] which has important implications for the design of efficient nanoantennas.

To explore the spectral differences between the near- and far-field properties of the nickel antennas, we performed further theoretical studies. We numerically calculated the far-field extinction (**Figure 6**a) and near-field amplitude spectra (Figure 6b) of different nickel disks of 60, 100, and 200 nm diameters on glass. The near-field spectra show the amplitude of the out-of-plane near-field component in a height of 20 nm above the disks. At $\lambda = 633$ nm wavelength, the near-field amplitude for the 100 and 200 nm diameter disks is comparably strong (Figure 6b), which is in good agreement with our experimental near-field measurements shown in Figure 5. More importantly, we find that the near-field resonance is dramatically redshifted compared to the far-field resonance. We note that earlier studies[33,34] with gold nanoantennas also report spectral shifts between the far-and near-field plasmon resonance, however, the relative spectral shifts for nickel disks are significantly larger.

The nature of the spectral shifts in plasmonic nanostructures is still a widely unexplored terrain, with only a few studies aiming at unveiling the underlying mechanism. To provide fundamental insights into the origin of this resonance shift, we study the simplest case of a plasmonic particle. We calculate the far-field extinction and near-field amplitude spectra of a small nickel sphere in the quasi-electrostatic approximation (Figure 6c), where we can exclude retardation, higher modes or radiation damping. We again find a significant shift between the two spectra, indicating that material intrinsic plasmon damping is the basic mechanism for this effect. To elucidate this phenomenon, we consider the dynamics of the plasmon being a strongly damped, forced harmonic oscillator[35] according to $\ddot{x} + \gamma\dot{x} + \omega_0^2 x = {}^{F}/_{m} \cos \Omega t$, where γ is the damping, ω_0 the eigenfrequency, F the driving force and m the mass.[36] The oscillator amplitude $A = \left[\left(\omega_0^2 - \Omega^2\right)^2 + \gamma^2\Omega^2\right]^{-1/2}$ can be associated with the near-field amplitude E_{loc}/E_{in}, and the energy dissipation of the oscillator $\Delta W = F^2\Omega^2\gamma / \left(2m\left[(\omega_0^2 - \Omega^2)^2 + \gamma^2\Omega^2\right]\right)$ can be associated to the far-field extinction cross section C_{ext}. As shown in Figure 6d, the maximum energy dissipation appears at the eigenfrequency ω_0, while the amplitude maximum is shifted to a lower frequency. The harmonic oscillator model thus clearly explains that the origin of the spectral shift between far- and near-field resonances in small nanostructures is essentially due to strong plasmon damping. This effect is particularly relevant in nickel antennas because of the large imaginary part of the dielectric function. We note that damping may not be the only factor causing the shift. In nanostructures of finite size, other effects may play a role. For example, it has been reported that with increasing structure size the spectral shift increases, which can be explained by additional damping caused by radiation losses.[34]

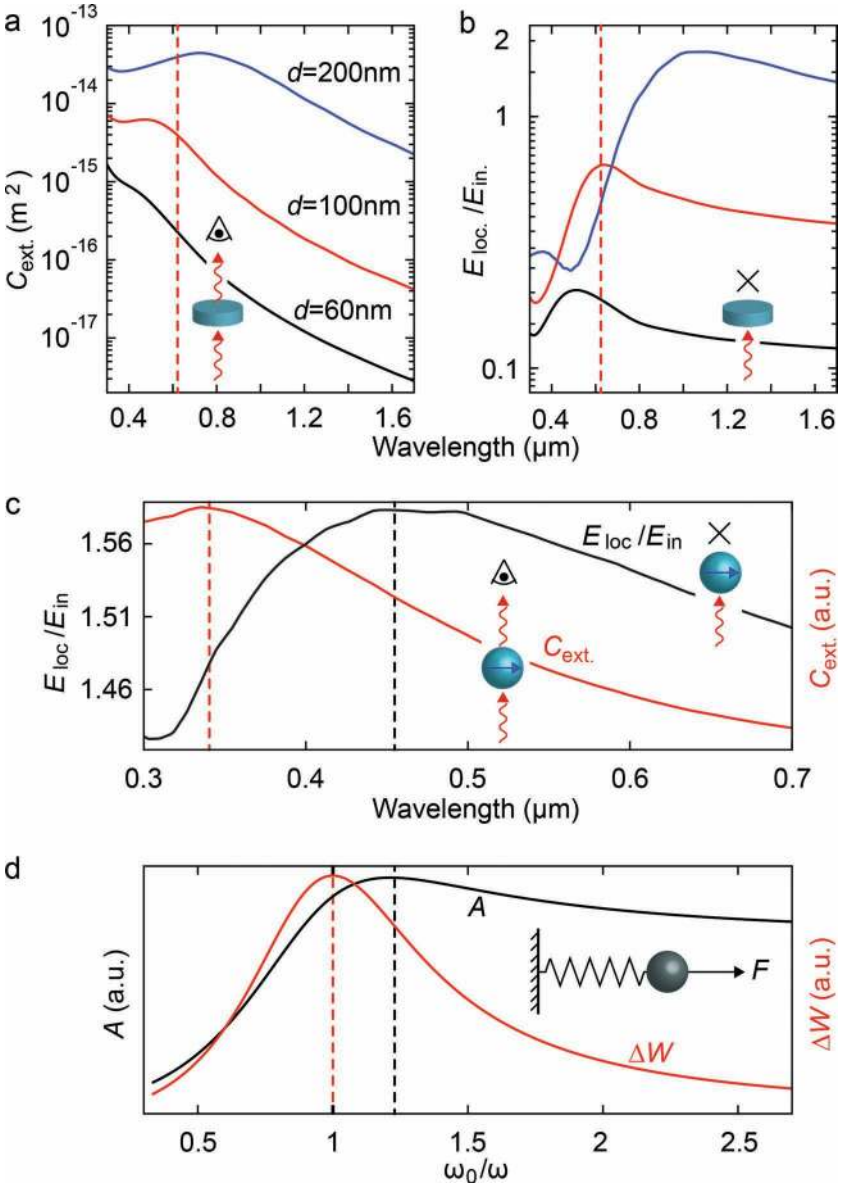

Figure 6. a) Calculated far-field extinction spectra C_{ext} and b) near-field spectra E_{loc}/E_{in} (out-of-plane component) of nickel disks of diameter $d = 60$, 100, 200 nm. The red dashed lines in (a) and (b) mark the near-field imaging wavelength. c) Calculated far-field extinction and near-field spectra of a small nickel sphere of diameter $d = 10$ nm. d) Calculated amplitude A and dissipation spectra ΔW according to the harmonic oscillator model.

3. Conclusion

In conclusion, this study provides direct experimental evidence of distinct dipolar plasmon modes in pure ferromagnetic nickel nanoantennas of different

sizes and shapes. The simultaneous ferromagnetic and plasmonic dual functionality of nickel opens interesting possibilities for novel applications, such as magnetic manipulation of the optical nanoantennas. Moreover, numerical calculations reveal significant differences between far- and near-field spectra of the nickel antennas, which are indicated by comparing single-wavelength near-field images and experimental far-field spectra. We find that the near-field resonance is dramatically red shifted compared to the far-field resonance, an effect that before has not been revealed so clearly in antennas made of standard noble metals. A simple harmonic oscillator model explains that plasmon damping is a major contribution to the shift between near- and far-field resonances. Owning to its strongly damped plasmon, nickel is a well-suited material to explore this phenomenon. Generally, the spectral difference between far- and near-field spectra is an interesting and fundamental property of plasmonic antennas. On the other hand, it needs to be taken into account when designing nanophotonic devices.

4. Experimental Section

The scattering-type scanning near-field optical microscope (*s*-SNOM) used in this work is based on an atomic force microscope (AFM) that uses cantilevered tips as near-field probes.[28] (Neaspec GmbH, www.neaspec.com). For antenna mode imaging we use standard commercial Si tips (Arrow tip, NanoWorld). The tip oscillates at the mechanical resonance frequency $\Omega \approx 300$ kHz with an amplitude of 30 nm, while the sample is scanned. A laser beam ($\lambda = 632.8$ nm) is focused to the tip apex using a parabolic mirror. The backscattered light is analyzed with a pseudo-heterodyne Michelson interferometer, yielding both the amplitude E and phase ϕ of the backscattered light.[28] Background contributions are suppressed by demodulating the detector signal at a harmonic frequency $n\Omega$ ($n \geq 2$), yielding background free near-field amplitude and phase images. In order to avoid distortion of the plasmon modes by near-field coupling between antenna and tip, we illuminate the sample with s-polarized light. In this scheme, the incident light efficiently polarizes the nickel antennas but not the AFM tip.[31,37,38] In the presented experiments, the p-polarized backscattered light is selected by a vertically aligned polarizer in front of the detector (Polarizer 1). To achieve interference between the s-polarized incident light and the detected p-polarized backscattered light, a 45 degree rotated polarizer (Polarizer 2) is placed in between the vibrating reference mirror and the beam splitter.

Acknowledgements

Supported by the European FP7 project 'Nanoantenna' (FP7-HEALTH-F5-2009-241818-NANOANTENNA) and the National Project MAT2009 –08398 from the Spanish Ministerio de Ciencia e Innovacion. J.A. acknowledges financial help by the Department of Industry of the Basque Government through the ETORTEK program NANOPHOT. P.V. acknowledges funding from the Basque Government under Programs No. PI2009–17 as well as the Spanish Ministry of Science and Education under Project No. MAT2009–07980. Z. P. acknowledges support from Swedish Foundation for Strategic Research through RMA08–0109 "Functional Electromagnetic Metamaterials" program. J. N. acknowledges funding from the Generalitat de Catalunya and the Spanish Ministry of Science and Education through No. 2009-SGR-1292 and No. MAT2010–20616-C02 projects. A.D. acknowledges support from the Swedish Research Council. Figure 4 and 5 were replaced with better quality images on August 22, 2011.

[1] K. B. Crozier, A. Sundaramurthy, G. S. Kino, C. F. Quate, *J. Appl. Phys.* **2003**, *94*, 4632.
[2] R. D. Grober, R. J. Schoelkopf, D. E. Prober, *Appl. Phys. Lett.* **1997**, *70*, 1354.
[3] P. Muhlschlegel, H. J. Eisler, O. J. F. Martin, B. Hecht, D. W. Pohl, *Science* **2005**, *308*, 1607.
[4] K. Kneipp, Y. Wang, H. Kneipp, L. T. Perelman, I. Itzkan, R. Dasari, M. S. Feld, *Phys. Rev. Lett.* **1997**, *78*, 1667.
[5] H. X. Xu, E. J. Bjerneld, M. Kall, L. Borjesson, *Phys. Rev. Lett.* **1999**, *83*, 4357.
[6] A. Kinkhabwala, Z. F. Yu, S. H. Fan, Y. Avlasevich, K. Mullen, W. E. Moerner, *Nat. Photonics* **2009**, *3*, 654.
[7] L. Novotny, R. X. Bian, X. S. Xie, *Phys. Rev. Lett.* **1997**, *79*, 645.
[8] A. J. Haes, W. P. Hall, L. Chang, W. L. Klein, R. P. Van Duyne, *Nano Lett.* **2004**, *4*, 1029.
[9] J. N. Anker, W. P. Hall, O. Lyandres, N. C. Shah, J. Zhao, R. P. Van Duyne, *Nat. Mater.* **2008**, *7*, 442.
[10] J. N. Farahani, D. W. Pohl, H. J. Eisler, B. Hecht, *Phys. Rev. Lett.* **2005**, *95*, 017402.
[11] T. H. Taminiau, F. D. Stefani, F. B. Segerink, N. F. Van Hulst, *Nat. Photonics* **2008**, *2*, 234.
[12] A. G. Curto, G. Volpe, T. H. Taminiau, M. P. Kreuzer, R. Quidant, N. F. van Hulst, *Science* **2010**, *329*, 930.
[13] A. Sundaramurthy, P. J. Schuck, N. R. Conley, D. P. Fromm, G. S. Kino, W. E. Moerner, *Nano Lett.* **2006**, *6*, 355.
[14] W. Srituravanich, N. Fang, C. Sun, Q. Luo, X. Zhang, *Nano Lett.* **2004**, *4*, 1085.
[15] E. Cubukcu, E. A. Kort, K. B. Crozier, F. Capasso, *Appl. Phys. Lett.* **2006**, *89*, 093120.
[16] N. Insin, J. B. Tracy, H. Lee, J. P. Zimmer, R. M. Westervelt, M. G. Bawendi, *ACS Nano* **2008**, *2*, 197.
[17] K. C. Weng, C. O. Noble, B. Papahadjopoulos-Sternberg, F. F. Chen, D. C. Drummond, D. B. Kirpotin, D. H. Wang, Y. K. Hom, B. Hann, J. W. Park, *Nano Lett.* **2008**, *8*, 2851.
[18] J. B. Gonzalez-Diaz, A. Garcia-Martin, G. Armelles, D. Navas, M. Vazquez, K. Nielsch, R. B. Wehrspohn, U. Gosele, *Adv. Mater.* **2007**, *19*, 2643.
[19] A. V. S. Ventsislav, K. Valev, Werner Gillijns, Yogesh Jeyaram, Hanna Paddubrouskaya, Alexander Volodin, Claudiu G. Biris, Nicolae C. Panoiu, Ben De Clercq, Marcel Ameloot, Oleg A. Aktsipetrov, Victor V. Moshchalkov, Thierry Verbiest, *ACS Nano* **2011**, *5*, 91.
[20] C. S. Levin, C. Hofmann, T. A. Ali, A. T. Kelly, E. Morosan, P. Nordlander, K. H. Whitmire, N. J. Halas, *ACS Nano* **2009**, *3*, 1379.
[21] N. J. Halas, *MRS Bull.* **2005**, *30*, 362.
[22] H. Wang, D. W. Brandl, P. Nordlander, N. J. Halas, *Accounts Chem. Res.* **2007**, *40*, 53.
[23] V. V. Temnov, G. Armelles, U. Woggon, D. Guzatov, A. Cebollada, A. Garcia-Martin, J. M. Garcia-Martin, T. Thomay, A. Leitenstorfer, R. Bratschitsch, *Nat. Photonics* **2010**, *4*, 107.
[24] J. D. Jackson, *Classical Electrodynamics*, John Wiley & Sons, New York **1975**.
[25] E. W. Palik, *Handbook of Optical Constants of Solids*, Academic, Orlando **1985**.

[26] H. Fredriksson, Y. Alaverdyan, A. Dmitriev, C. Langhammer, D. S. Sutherland, M. Zaech, B. Kasemo, *Adv. Mater.* **2007**, *19*, 4297.
[27] P. Vavassori, *Appl. Phys. Lett.* **2000**, *77*, 1605.
[28] N. Ocelic, A. Huber, R. Hillenbrand, *Appl. Phys. Lett.* **2006**, *89*, 101124.
[29] M. Schnell, A. Garcia-Etxarri, J. Alkorta, J. Aizpurua, R. Hillenbrand, *Nano Lett.* **2010**, *10*, 3524.
[30] R. Hillenbrand, F. Keilmann, P. Hanarp, D. S. Sutherland, J. Aizpurua, *Appl. Phys. Lett.* **2003**, *83*, 368.
[31] R. Esteban, R. Vogelgesang, J. Dorfmuller, A. Dmitriev, C. Rockstuhl, C. Etrich, K. Kern, *Nano Lett.* **2008**, *8*, 3155.
[32] S. Link, M. A. El-Sayed, *J. Phys. Chem. B* **1999**, *103*, 8410.
[33] G. W. Bryant, F. J. G. De Abajo, J. Aizpurua, *Nano Lett.* **2008**, *8*, 631.
[34] B. M. Ross, L. P. Lee, *Opt. Lett.* **2009**, *34*, 896.
[35] J. Zuloaga, P. Nordlander, *Nano Lett.* **2011**, *11*, 1280.
[36] D. R. H. Craig, F. Bohren, *Absorption and Scattering of Light by Small Particles*, John Wiley & Sons, New York **1998**.
[37] D. S. Kim, J. Heo, S. H. Ahn, S. W. Han, W. S. Yun, Z. H. Kim, *Nano Lett.* **2009**, *9*, 3619.
[38] M. Rang, A. C. Jones, F. Zhou, Z. Y. Li, B. J. Wiley, Y. Xia, M. B. Raschke, *Nano Lett.* **2008**, *8*, 3357.

Received: April 3, 2011
Published online: June 16, 2011